PHYSICAL REVIEW D **95,** 074506 (2017)

Effects of boundary conditions and gradient flow in (1 + 1)-dimensional lattice ϕ^4 theory

A. Harindranath[1,*] and Jyotirmoy Maiti[2,†]

[1]*Theory Division, Saha Institute of Nuclear Physics 1/AF Bidhan Nagar, Kolkata 700064, India*
[2]*Department of Physics, Tehatta Government College, Tehatta, Nadia, West Bengal 741160, India*

(Received 4 January 2017; published 13 April 2017)

In this work we study the effects of boundary conditions and gradient flow in 1 + 1-dimensional lattice ϕ^4 theory. Simulations are performed with periodic (PBC) and open (OPEN) boundary conditions in the temporal direction and the lattice fields are then smoothed by applying gradient flow. Our results for observables—such as $\langle|\phi|\rangle$ and the susceptibility—indicate that at a given volume the phase transition point is shifted towards a lower value of the lattice coupling λ_0 for a fixed m_0^2 in the case of OPEN compared to PBC, and the shift decreases as the volume increases. We employ the finite-size scaling (FSS) analysis to obtain the true critical behavior, mainly to emphasize the necessity of a FSS formalism incorporating the surface effect in the case of the open boundary. The above features are found to be illuminated more clearly by the application of gradient flow. Finally, we compare and contrast the extraction of the boson mass from the two-point function (PBC) and the one-point function (OPEN) as the coupling (starting from moderate values) approaches the critical value corresponding to the vanishing of the mass gap. In the critical region, finite-volume effects become dominant in the latter. The surface effect seems to result in a less sharp phase transition for OPEN compared to PBC for all observables studied here.

DOI: 10.1103/PhysRevD.95.074506

I. INTRODUCTION AND MOTIVATION

The quantum field theory of the 1 + 1-dimensional ϕ^4 interaction, in spite of its apparent simplicity, has a very rich structure and hence has been the testing ground for various new nonperturbative approaches towards the field theory. It also provides ample opportunity to study newly proposed algorithms and calculational techniques. Extensive numerical results have been presented in this theory in an earlier work [1]. In this work we present numerical studies in this theory in the context of comparison between periodic (PBC) and open boundary conditions (OPEN) in the temporal direction and the effects of gradient flow (also known as Wilson flow).

In addition to the periodic boundary conditions in both the temporal and spatial directions, one can have other types of boundary conditions. For the scalar field, for example, one can have antiperiodic boundary conditions in the spatial direction. In the latter case one can study quantum kinks [2]. Lattice quantum chromodynamics (LQCD) conventionally uses PBC in both the temporal and spatial directions for the gauge field. However, in this case, the spanning of gauge configurations over different topological sectors becomes more and more difficult as the continuum limit is approached. As a remedy, an open boundary condition in the temporal direction has been proposed [3–5]. Numerical studies in pure Yang-Mills theory [6–10] and QCD [11] have yielded encouraging results.

In order for OPEN to be effective, boundary artifacts should be negligible so that one has a bulk region of considerable extent. This is possible as long the system is not gapless (critical) [12]. The success of OPEN in pure Yang-Mills theory and QCD hinges on the existence of a mass gap in these systems, namely, a glueball and pion, respectively. On the other hand, 1 + 1-dimensional lattice ϕ^4 theory offers an opportunity to investigate in detail the artifacts induced by the open boundary condition as the system approaches criticality.

To extract various observables in lattice field theories, smoothing the lattice fields is essential in order to overcome lattice artifacts. The gradient (Wilson) flow [13–15] provides a very convenient tool for smoothing, with a rigorous mathematical underpinning. For some recent studies of gradient flow in the context of scalar theory, see Refs. [16–19]. In our previous work on Yang-Mills theory, we have demonstrated the effectiveness of gradient flow in the extraction of the topological susceptibility and glueball masses. Thus it will be very interesting to study the effect of gradient flow on various observables, independent of the boundary condition, in 1 + 1-dimensional lattice ϕ^4 theory.

II. BOUNDARY CONDITIONS AND GRADIENT FLOW

In the continuum, the Euclidean Lagrangian (density) for ϕ^4 theory is given by

$$\mathcal{L} = \frac{1}{2}\partial_\mu\phi\partial_\mu\phi + \frac{1}{2}m^2\phi^2 + \frac{\lambda}{4!}\phi^4. \tag{1}$$

*a.harindranath@saha.ac.in
†jyotirmoy.maiti@gmail.com

 © 2017 American Physical Society

On a periodic (in all space-time directions) lattice, the Euclidean action in d space-time dimensions is conventionally written as [1]

$$S = -\sum_x \sum_\mu \tilde{\phi}_x \tilde{\phi}_{x+\mu} + \left(d + \frac{m_0^2}{2}\right) \sum_x \tilde{\phi}_x^2 + \frac{\lambda_0}{4!} \sum_x \tilde{\phi}_x^4, \quad (2)$$

where all the parameters and fields have been made dimensionless by multiplying them with appropriate powers of the lattice spacing a.

However, in order to impose the open boundary condition in the temporal direction we follow the construction of the transfer matrix. For this purpose the lattice action is written in terms of time-slice action density $E(t)$ as $S = \sum_t E(t)$ and the kinetic term in the temporal direction is distributed symmetrically around the time slice t. The details are given below.

First, with the aid of forward and backward lattice derivatives

$$\partial_\mu^f \phi = \frac{1}{a}(\phi_{x+\mu} - \phi_x) \quad \text{and} \quad \partial_\mu^b \phi = \frac{1}{a}(\phi_x - \phi_{x-\mu}), \quad (3)$$

we write the symmetrized expression for the kinetic term as

$$\begin{aligned} &\frac{1}{2}\partial_\mu \phi \partial_\mu \phi \\ &= \frac{1}{4}(\partial_\mu^f \phi \partial_\mu^f \phi + \partial_\mu^b \phi \partial_\mu^b \phi) \\ &= \frac{1}{4a^2}\left(2\sum_\mu \phi_x^2 + \phi_{x+\mu}^2 + \phi_{x-\mu}^2 - 2\phi_x \phi_{x+\mu} - 2\phi_x \phi_{x-\mu}\right). \end{aligned} \quad (4)$$

This enables one to write down the time-slice action density for the periodic lattice as

$$E_{\mathrm{PBC}}(t) = \mathcal{T}_t + \mathcal{V}_t + \frac{1}{2}\mathcal{T}_{t,t+1} + \frac{1}{2}\mathcal{T}_{t-1,t}, \quad (5)$$

where

$$\begin{aligned} \mathcal{V}_t &= \sum_{\vec{x}} \left(\frac{1}{2}a^2 m^2 \phi_{\vec{x},t}^2 + \frac{a^2\lambda}{4!}\phi_{\vec{x},t}^4\right), \\ \mathcal{T}_t &= \frac{1}{4}\sum_{\vec{x},k}(2\phi_{\vec{x},t}^2 + \phi_{\vec{x}+\hat{k},t}^2 + \phi_{\vec{x}-\hat{k},t}^2 \\ &\quad - 2\phi_{\vec{x},t}\phi_{\vec{x}+\hat{k},t} - 2\phi_{\vec{x},t}\phi_{\vec{x}-\hat{k},t}), \\ \mathcal{T}_{t,t+1} &= \frac{1}{2}\sum_{\vec{x}}(\phi_{\vec{x},t}^2 + \phi_{\vec{x},t+1}^2 - 2\phi_{\vec{x},t}\phi_{\vec{x},t+1}), \\ \mathcal{T}_{t-1,t} &= \frac{1}{2}\sum_{\vec{x}}(\phi_{\vec{x},t}^2 + \phi_{\vec{x},t-1}^2 - 2\phi_{\vec{x},t}\phi_{\vec{x},t-1}), \end{aligned}$$

with $\hat{k}$ being the unit vector in an arbitrary spatial direction.

Following this definition, we denote $e^{-H_m(t,t+1)}$ as the general transfer matrix element between the time slices t and $t+1$, where

$$H_m(t,t+1) = \frac{1}{2}(\mathcal{T}_t + \mathcal{V}_t) + \frac{1}{2}(\mathcal{T}_{t+1} + \mathcal{V}_{t+1}) + \mathcal{T}_{t,t+1}. \quad (6)$$

In particular, for a lattice of temporal extent T the transfer matrix element between the boundary time slices $t = T-1$ and $t = 0$ is determined by

$$H_m(T-1,0) = \frac{1}{2}(\mathcal{T}_{T-1} + \mathcal{V}_{T-1}) + \frac{1}{2}(\mathcal{T}_0 + \mathcal{V}_0) + \mathcal{T}_{T-1,0}.$$

Now, if the temporal boundary becomes open, the corresponding term drops out from the partition function. This leads us to relate the actions for lattices with two different boundary conditions in the temporal direction (periodic and open) as $S_{\mathrm{PBC}} = S_{\mathrm{OPEN}} + \Delta S$, where $\Delta S = H_m(T-1,0)$.

The absence of the term ΔS from the action for a lattice with an open boundary (temporal direction), in turn, also modifies the expressions for the action densities at the temporal boundaries. They are given by

$$E_{\mathrm{OPEN}}(t=0) = \frac{1}{2}(\mathcal{T}_0 + \mathcal{V}_0) + \frac{1}{2}\mathcal{T}_{0,1} \quad (7)$$

$$\text{and} \quad E_{\mathrm{OPEN}}(t=T-1) = \frac{1}{2}(\mathcal{T}_{T-1} + \mathcal{V}_{T-1}) + \frac{1}{2}\mathcal{T}_{T-2,T-1}. \quad (8)$$

Within the bulk ($0 < t < T-1$), $E_{\mathrm{OPEN}}(t) = E_{\mathrm{PBC}}(t)$.

In order to smooth the lattice ϕ field, gradient flow is used. For ϕ^4 theory it is known that, in four dimensions, there are potential divergences in the correlation functions for a flow time greater than zero, and for this reason in Refs. [16] and [18] a simple flow equation corresponding to the free-field theory was used. Fujikawa [17] proposed a modification of the flow equation to tackle this problem. However, the ϕ^4 in $1+1$ dimensions which we study here is free from such divergences. Here we follow the choice made in our previous works for Yang-Mills theory, namely, picking the gradient of the action to drive the flow. Thus, for ϕ^4 theory in Euclidean space in $1+1$ dimensions, in the continuum the flow equation is chosen to be

$$\begin{aligned} \frac{\partial \psi(x,\tau)}{\partial \tau} &= -\frac{\delta S[\psi]}{\delta \psi(x,\tau)} \\ &= \partial_\mu \partial_\mu \psi(x,\tau) - m^2 \psi(x,\tau) - \frac{\lambda}{6}\psi^3(x,\tau), \end{aligned} \quad (9)$$

where $\psi(x,\tau=0) = \phi(x)$, with τ being the flow time.

We numerically solve this equation on the lattice using the second-order Runge-Kutta method.

III. EXTRACTION OF BOSON MASS FROM LATTICES WITH DIFFERENT BOUNDARIES

For the extraction of boson mass we use the simplest and most familiar scalar operator: the time-sliced field $\phi(t) = \frac{1}{V}\sum_{\vec{x}}\phi(\vec{x}, t)$, where V is the spatial volume of the lattice. The mass can be easily extracted from the two-point correlation function for this scalar operator which, in the case of a periodic boundary in the temporal direction, behaves as

$$G(t) = \langle\phi(t)\phi(t=0)\rangle_{\mathrm{PBC}} \approx C_0 + C_1[e^{-mt} + e^{-m(T-t)}] = C_0 + 2C_1 e^{-mT/2}\cosh m\left(\frac{T}{2} - t\right), \tag{10}$$

where

$$C_1 = \frac{|\langle 0|\phi(0)|B\rangle|^2}{2m}, \tag{11}$$

with $|B\rangle$ being the one-boson state. To improve statistics, one can average over the source time as well. The effective mass can be evaluated by solving the equation $F(m) = 0$,

$$\text{where } F(m) = (r_1 - 1)[\cosh m(\Delta t - 1) - \cosh m\Delta t] + (1 - r_2)[\cosh m(\Delta t + 1) - \cosh m\Delta t], \tag{12}$$

$$\text{with} \quad r_1 = \frac{G(t-1)}{G(t)}, \qquad r_2 = \frac{G(t+1)}{G(t)}, \quad \text{and} \quad \Delta t = T/2 - t. \tag{13}$$

Note that the boson mass extracted from the propagator using Eq. (10) is the pole mass and hence is the physical mass [20], independent of the lattice spacing.

In the case of an open boundary in the time direction, to avoid the boundary effects one needs to be well within the bulk while computing the two-point correlation function. However, the second exponential will be absent from the expression for the two-point function due to the loss of periodicity. On the other hand, as the time translational invariance is also lost in this case, one cannot average over the source time as well. However, within the bulk, well away from the boundary region translational invariance is recovered. So one can take the average over a few time slices to regain statistics.

However, this effort breaks down as one approaches the critical region. It will be shown later on in this study that the effect of an open boundary starts to engulf the whole bulk region as we move towards the critical point. Mass extraction from the two-point function becomes almost impossible.

Surprisingly, the open boundary itself opens up new pathways to extract the mass. Following Ref. [9], in this section we review how the boson mass can be extracted from a one-point function in the case of an open boundary using a generic time-sliced scalar operator $\mathcal{O}(t)$.

We start from

$$\begin{aligned}\langle\mathcal{O}(t)\rangle_{\mathrm{OPEN}} &= \frac{\int \mathcal{D}\phi\mathcal{O}(t)e^{-S_{\mathrm{OPEN}}}}{\int \mathcal{D}\phi e^{-S_{\mathrm{OPEN}}}} \\ &= \frac{\int \mathcal{D}\phi\mathcal{O}(t)e^{-S_{\mathrm{PBC}}+\Delta S}/\int \mathcal{D}\phi e^{-S_{\mathrm{PBC}}}}{\int \mathcal{D}\phi e^{-S_{\mathrm{PBC}}+\Delta S}/\int \mathcal{D}\phi e^{-S_{\mathrm{PBC}}}} \\ &= \langle\mathcal{O}(t)\rangle_{\mathrm{PBC}} + \frac{\langle\mathcal{O}(t)e^{\Delta S}\rangle^{\mathrm{connected}}_{\mathrm{PBC}}}{\langle e^{\Delta S}\rangle_{\mathrm{PBC}}} \qquad (14) \\ &= \langle\mathcal{O}(t)\rangle_{\mathrm{PBC}} + \frac{1}{r}\langle\mathcal{O}(t)e^{H_m(T-1,0)}\rangle^{\mathrm{connected}}_{\mathrm{PBC}}, \qquad (15)\end{aligned}$$

where $r = \langle e^{\Delta S}\rangle_{\mathrm{PBC}} = \langle e^{H_m(T-1,0)}\rangle_{\mathrm{PBC}}$. As $e^{H_m(t,t+1)}$ is also a scalar operator, from Eq. (15) we have

$$\langle\mathcal{O}(t)\rangle_{\mathrm{OPEN}} \approx \langle\mathcal{O}(t)\rangle_{\mathrm{PBC}} + 2C_1' e^{-mT/2}\cosh m\left(\frac{T}{2} - t\right), \tag{16}$$

where m is the scalar boson mass.

Thus we find that one can extract certain two-point correlators computed with the periodic boundary condition in the temporal direction by analyzing the data for the functional average of a scalar operator (one-point function) computed with an open boundary (in the temporal direction) in the region of t where it differs (due to the breaking of translational invariance) from the same computed with a periodic boundary. Now due to time translational invariance in the case of PBC, we can assume $\langle\mathcal{O}(t)\rangle_{\mathrm{PBC}}$ to be constant and the evaluation of the effective mass can then be done again following Eqs. (12) and (13).

IV. SIMULATION DETAILS

As we have restricted ourselves to $1+1$ dimensions within this study, the fields are dimensionless here. The notations for the bare parameters of the theory on the lattice are chosen to be $m_0^2 = a^2m^2$ and $\lambda_0 = a^2\lambda$. As we know, for the stability of the theory one must have $\lambda_0 \geq 0$ and the phase transition associated with the spontaneous breaking (or restoration) of $Z(2)$ symmetry takes place only for $m_0^2 < 0$.

For the study with a periodic boundary in both directions, following the method of Brower and Tamaya [21], we have used Wolff's single cluster algorithm [22,23] blended with the standard metropolis algorithm in a 1:1 ratio for the generation of field configurations. For the details of the whole procedure, see Ref. [1]. However, in the study with an open boundary in the temporal direction (periodic in the

spatial direction), we resort only to the standard metropolis algorithm for configuration generation.

Following the discussions in Ref. [1], we use $\langle|\phi|\rangle$ as the order parameter to investigate the phase structure. Here, $\phi = \sum_{\text{sites } x}\phi(x)/\text{lattice volume}$. The absolute value is taken to avoid the effect of tunneling enforced by the algorithm of configuration generation. For the phase diagram we mainly resort to the former study [1]. Here, we will study the effects of gradient flow and boundary conditions on the phase diagram in due course.

In this work, we explore the phase structure and the spectrum of the theory for two different sets of bare parameters given by $m_0^2 = -0.5$ and $m_0^2 = -1.0$. For each set of parameters (i.e., m_0^2 and λ_0), we first discard 10^6 configurations for thermalization and then generate another 10^8 configurations to perform the measurement. Measurements are done on one in every one thousand configurations. In order to study the finite-size effects on the results, whole investigations are done with four different lattice volumes, such as 48^2, 64^2, 96^2, and 128^2.

Configurations chosen for measurements are placed under gradient flow which is run for one hundred steps—which we call as flow level—with a step size of $\delta\tau = 0.02$. Measurements are done after every ten flow levels in addition to the measurement done before the flow is started.

V. NUMERICAL RESULTS

In this section we present and discuss our numerical results which show the effects of the boundary conditions and the gradient flow on various observables of interest. In principle, one could divide this into two separate studies altogether as the gradient flow and the boundary condition are two completely disjoint categories. Neither of them has anything to do with the other. However, on the one hand we

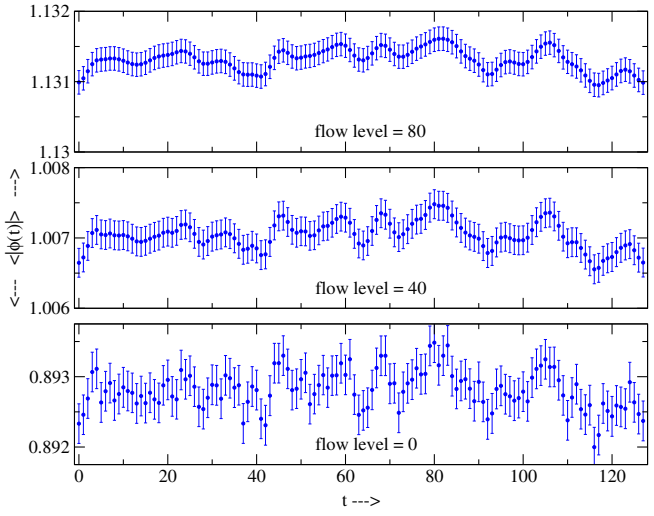

FIG. 1. Plot of the expectation value of $|\phi(t)|$ for $m_0^2 = -0.5$, $\lambda_0 = 1.65$, and $L = 128$ with PBC for three different gradient flow levels.

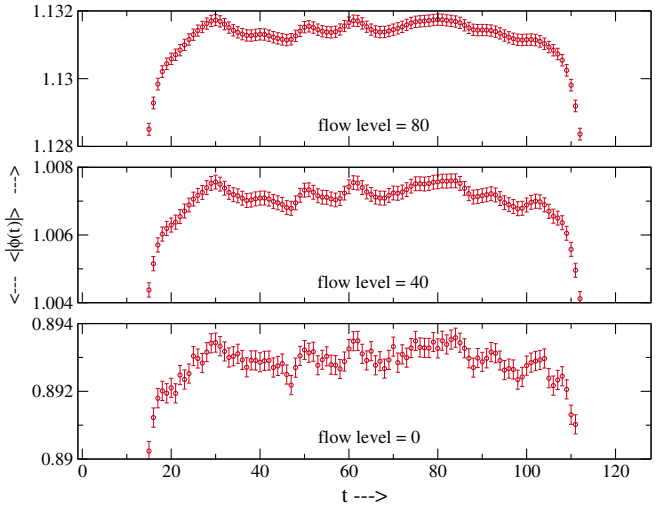

FIG. 2. Plot of the expectation value of $|\phi(t)|$ for $m_0^2 = -0.5$, $\lambda_0 = 1.65$, and $L = 128$ with OPEN for three different levels of gradient flow.

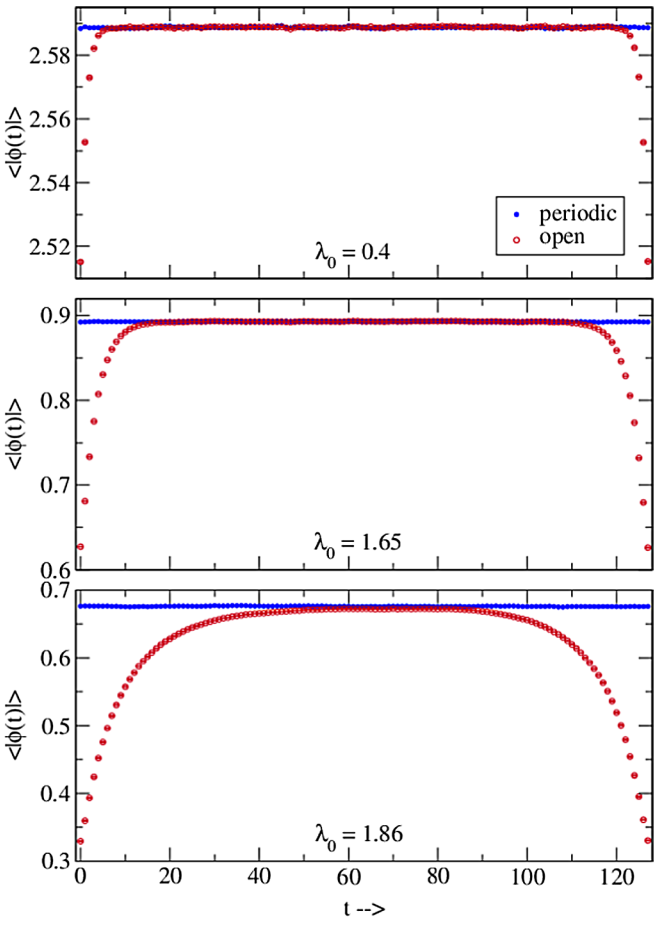

FIG. 3. Comparison of $\langle|\phi(t)|\rangle$ between PBC and OPEN for $m_0^2 = -0.5$, $L = 128$, and three different values of λ_0 without any gradient flow.

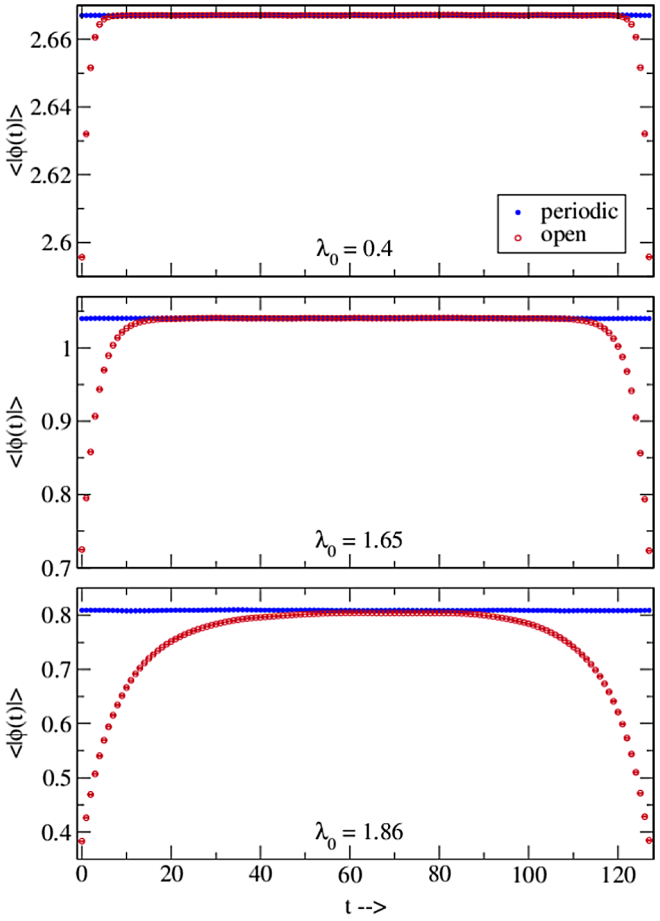

FIG. 4. Comparison of $\langle|\phi(t)|\rangle$ between PBC and OPEN for $m_0^2 = -0.5$, $L = 128$, and three different values of λ_0 at gradient flow level 50.

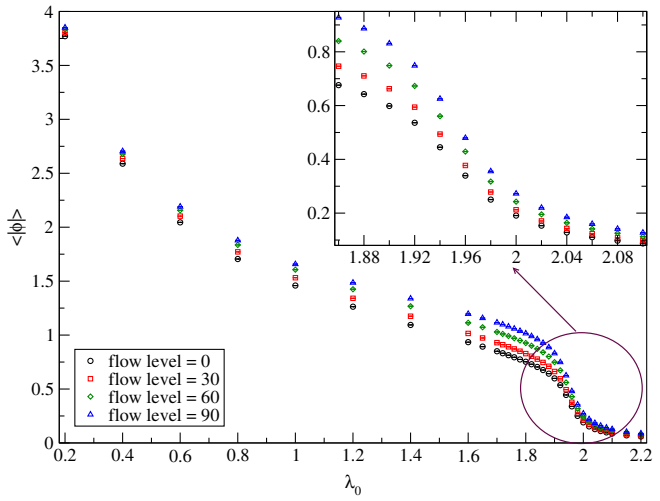

FIG. 5. Plot of $\langle|\phi|\rangle$ versus λ_0 for different values of the gradient flow level for $m_0^2 = -0.5$ and $L = 128$ in the case of PBC.

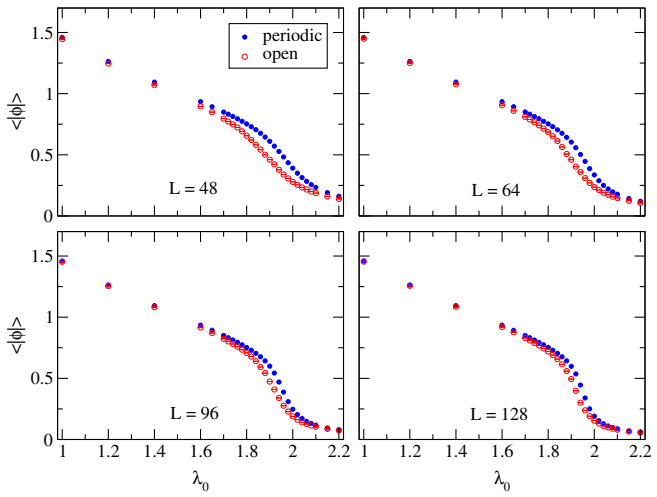

FIG. 6. Plot of $\langle|\phi|\rangle$ versus λ_0 for PBC and OPEN without gradient flow for different L at $m_0^2 = -0.5$.

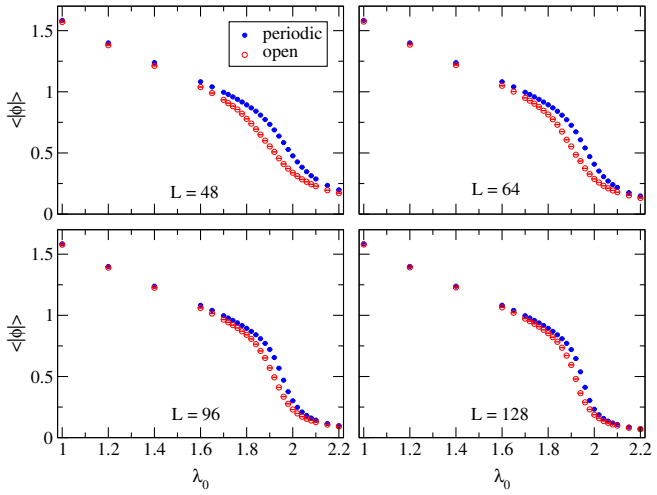

FIG. 7. Plot of $\langle|\phi|\rangle$ versus λ_0 for PBC and OPEN at gradient flow level 50 for different L at $m_0^2 = -0.5$.

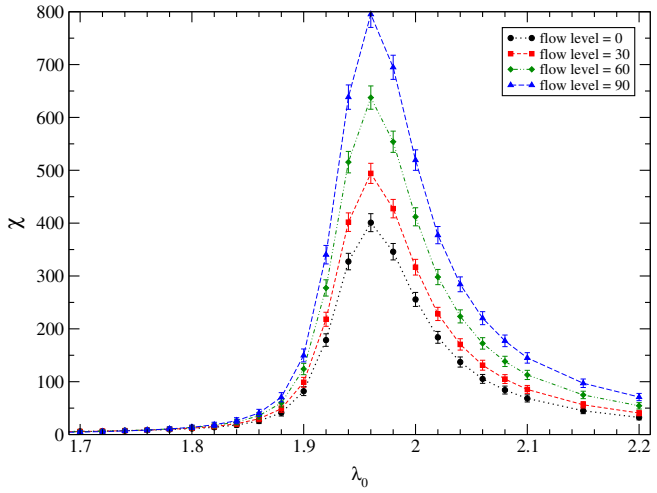

FIG. 8. Comparison of the susceptibility for different levels of gradient flow with PBC at $m_0^2 = -0.5$ and $L = 128$.

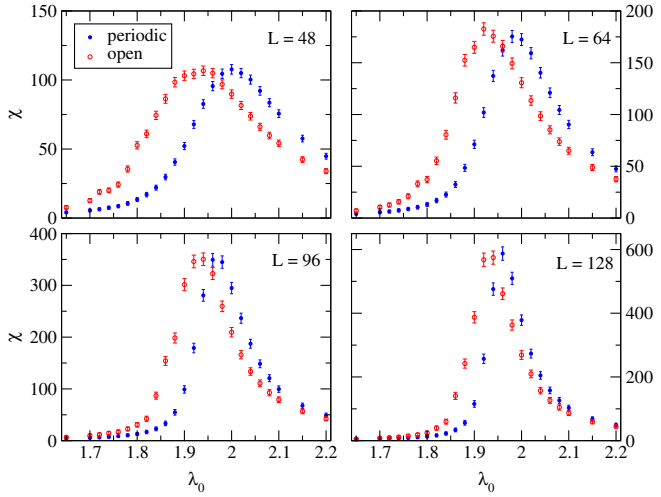

FIG. 9. Comparison of the susceptibility between PBC and OPEN for different L at $m_0^2 = -0.5$ and gradient flow level 50.

want to study the smoothening utility of the gradient flow irrespective of the choice of the boundary condition, and on the other hand we have a different aim to study the effect of the boundary condition as well. Thus they have come together in the same discussion here. Nevertheless, they are independent of each other.

A. The field variable

As the translational invariance is lost in the temporal direction when the open boundary condition is imposed in that direction, the time-sliced scalar field $\phi(t)$ could serve as an important observable to study the effect of an open boundary as compared to a periodic boundary. For the reasons stated earlier, here also we take the absolute value before evaluating the configuration average.

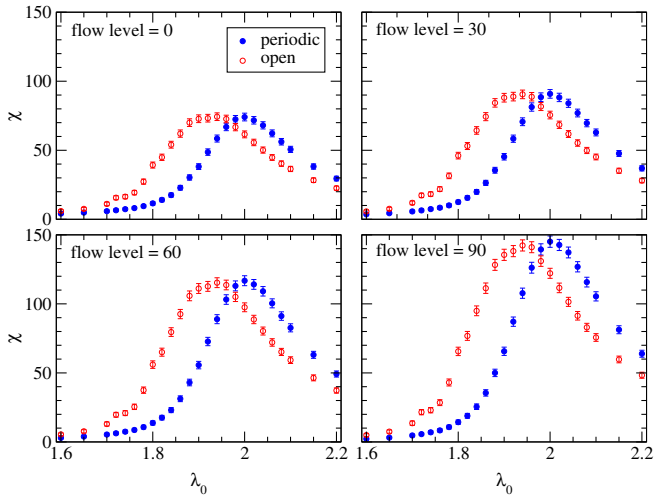

FIG. 10. Comparison of the susceptibility between PBC and OPEN for different levels of gradient flow at $m_0^2 = -0.5$ with $L = 48$.

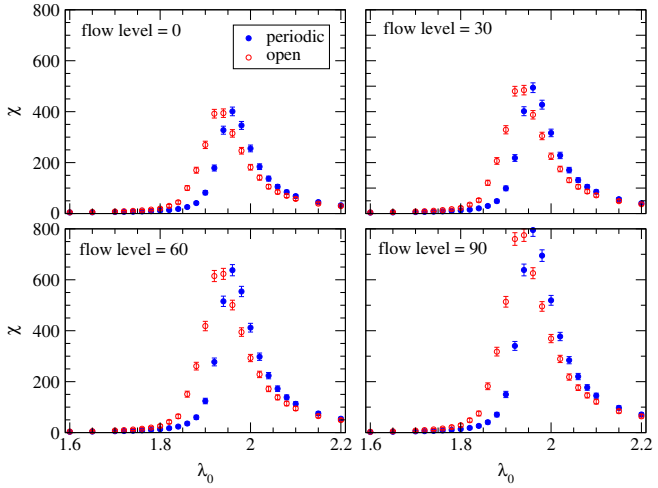

FIG. 11. Comparison of the susceptibility between PBC and OPEN for different levels of gradient flow at $m_0^2 = -0.5$ with $L = 128$.

In Figs. 1 and 2 for periodic and open boundary conditions in temporal directions, respectively, we present the expectation value of $|\phi(t)|$ in three different subdiagrams—one without any gradient flow, and two others with two different levels of

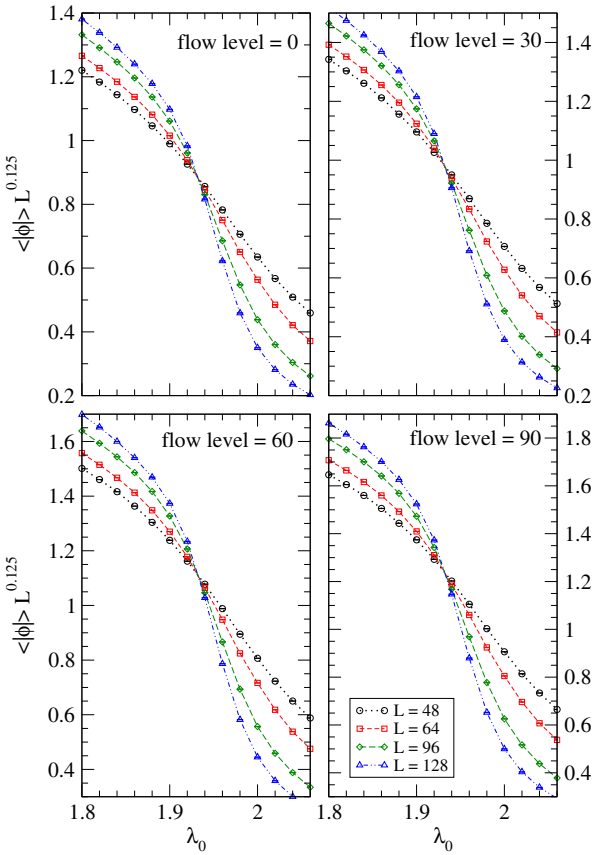

FIG. 12. Plot of $\langle|\phi|\rangle L^{0.125}$ versus λ_0 for different levels of gradient flow with PBC at $m_0^2 = -0.5$.

gradient flow—all for a particular set of lattice parameters $m_0^2 = 0.5$, $\lambda_0 = 1.65$, and a 128^2 lattice. The figures clearly show the smoothening effect with the increase of flow level. Note that the values of $\langle|\phi(t)|\rangle$ gradually increase with increasing flow level. The widths of the windows for the values of $\langle|\phi(t)|\rangle$ are taken to be the same in all three subdiagrams, instead of taking them to be proportional to the respective average values. This actually has reduced the manifestation of the smoothening effect to some extent.

To make the exhibition of the boundary effect clearer, in Fig. 3 we compare the behavior of $\langle|\phi(t)|\rangle$ for $m_0^2 = -0.5$ and $L = 128$ for periodic and open boundary conditions without any gradient flow for three different values of λ_0, all in the broken symmetric phase. For the smallest value of the coupling which is far away from the critical point the effects of the open boundary are only found at the edges, leaving a long bulk region that matches the counterpart in PBC. As the coupling increases one gets closer to the region of the phase transition and the effect of the open boundary extends on both side, squeezing the bulk. For $\lambda_0 = 1.86$, we are already in the critical region and we observe that the bulk region has almost vanished. The same is presented in Fig. 4 for gradient flow level 50. We notice that it only smoothens the data [although it is hardly visible here because of the wide scale of values for $\langle|\phi(t)|\rangle$ covered in the figure], leaving the boundary effects unchanged.

In Fig. 5 we plot $\langle|\phi|\rangle$ versus λ_0 for different values of the gradient flow level for a 128^2 lattice at $m_0^2 = -0.5$. The monotonous rise in the value of $\langle|\phi|\rangle$ with increasing gradient flow level is consistent with the behavior of $\langle|\phi(t)|\rangle$. Details of the behavior in the critical region are shown in the inset of the figure. The trend seems to be retained across the phase transition, with the additional feature of a sharper decrease of the observable across the transition point as the flow level is increased.

In Fig. 6, we present the comparison between $\langle|\phi|\rangle$ computed using PBC and the same obtained with OPEN for different lattice sizes at $m_0^2 = -0.5$ before applying the gradient flow on the fields. Deep in both the broken-symmetric and the symmetric phases, for all the lattice volumes, the results for PBC and OPEN are found to match within our statistical error. However, inside the critical region a clear disagreement is observed. A phase transition appears to take place at smaller values of λ_0 in the case of OPEN compared to PBC. However, the gap between the transition point in the two different boundaries seems to be vanishing as the lattice size increases. In addition, although not clearly prominent, it appears that the fall of $\langle|\phi|\rangle$ across

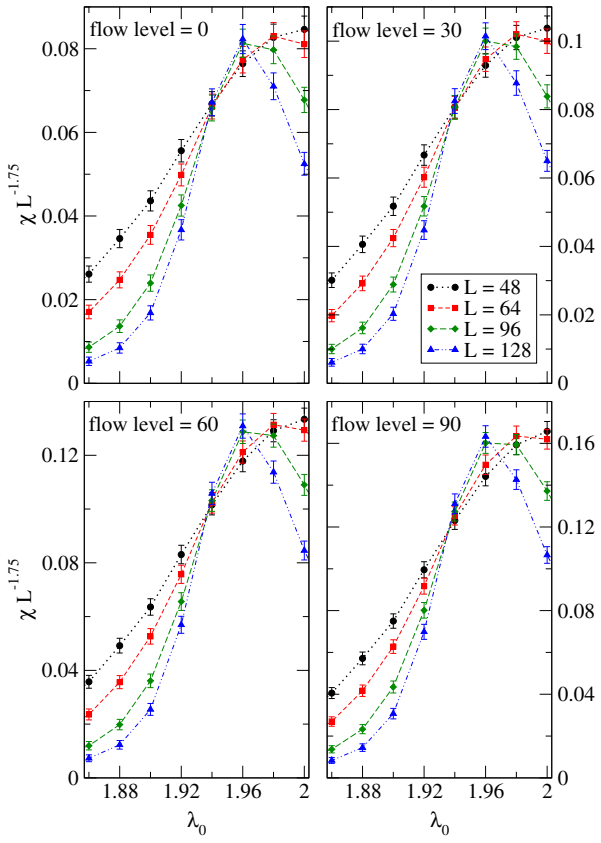

FIG. 13. Plot of $\chi L^{-1.75}$ versus λ_0 for different levels of gradient flow with PBC at $m_0^2 = -0.5$.

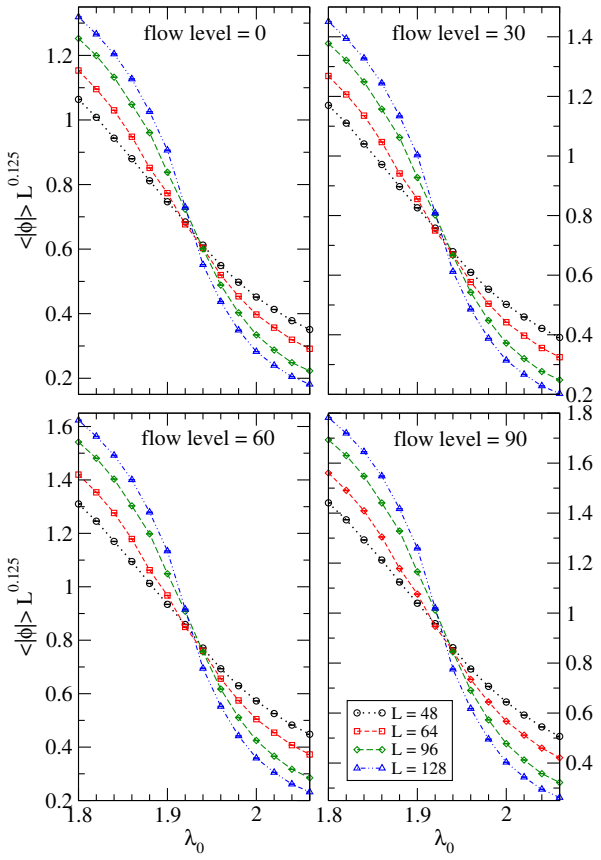

FIG. 14. Plot of $\langle|\phi|\rangle L^{0.125}$ versus λ_0 for different levels of gradient flow at $m_0^2 = -0.5$ with an open boundary.

the transition point is slightly sharper for PBC in comparison with OPEN. Both these behaviors are consistent with the expectation that the effect of the boundary surface diminishes in the infinite-volume limit. The picture is unaltered by the application of gradient flow other than slightly raising all of the values. This is shown in Fig. 7.

B. The susceptibility

In this subsection, we study the effects of gradient flow and the boundary conditions on the behavior of another observable of interest, namely, the susceptibility defined as $\chi = \sum_x \langle \phi(x)\phi(0)\rangle$/lattice volume. In Fig. 8, we show the behavior of the susceptibility as a function of λ_0 for $m_0^2 = -0.5$ with PBC on a 128^2 lattice for different levels of gradient flow. Consistent with the trends observed in the case of $\langle|\phi|\rangle$, the peak of the susceptibility becomes higher and higher as the level of gradient flow increases, leaving the peak position unchanged. This behavior is expected since the gradient flow serves to remove the lattice artifacts and brings the lattice theory closer to the continuum limit.

Analogous to the study done for $\langle|\phi|\rangle$, we compare the susceptibility between the periodic and open boundary conditions for different lattice sizes (L) at $m_0^2 = -0.5$ and gradient flow level 50 in Fig. 9. Here also we observe that, compared to the case of PBC, the peak is shifted towards the smaller values of λ_0 in the case of OPEN at a fixed L and the magnitude of the shift decreases as L increases.

This shift in the peak position of the susceptibility between PBC and OPEN seems to be unaffected by gradient flow as per our expectation. This has been demonstrated in Figs. 10 and 11 for the smallest and largest lattice sizes ($L = 48$ and $L = 128$, respectively), both with $m_0^2 = -0.5$.

From all the figures here comparing the susceptibility between PBC and OPEN, it appears that the peak is slightly sharper in the case of the former compared to the latter, consistent with the case of $\langle|\phi|\rangle$.

C. Finite-size scaling analysis

The fact that the value of $\langle|\phi|\rangle$ changes with gradient flow even in the critical region raises an interesting question. Is the determination of the critical coupling in a finite-size scaling (FSS) analysis affected by gradient flow? Here we study the possible effect of gradient flow in the FSS of the data for $\langle|\phi|\rangle$ to determine the critical coupling. We follow the discussion of the main aspects of finite-size scaling [24–26] given in Ref. [1]. FSS assumes that, in a finite system, out of the three length scales involved—namely, the correlation length ξ, the size of the

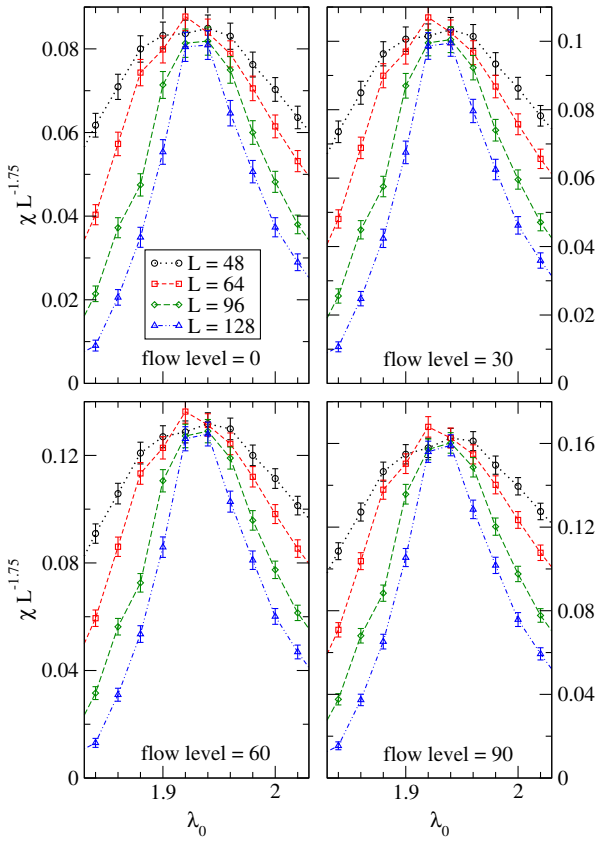

FIG. 15. Plot of $\chi L^{-1.75}$ versus λ_0 for different levels of gradient flow at $m_0^2 = -0.5$ with an open boundary.

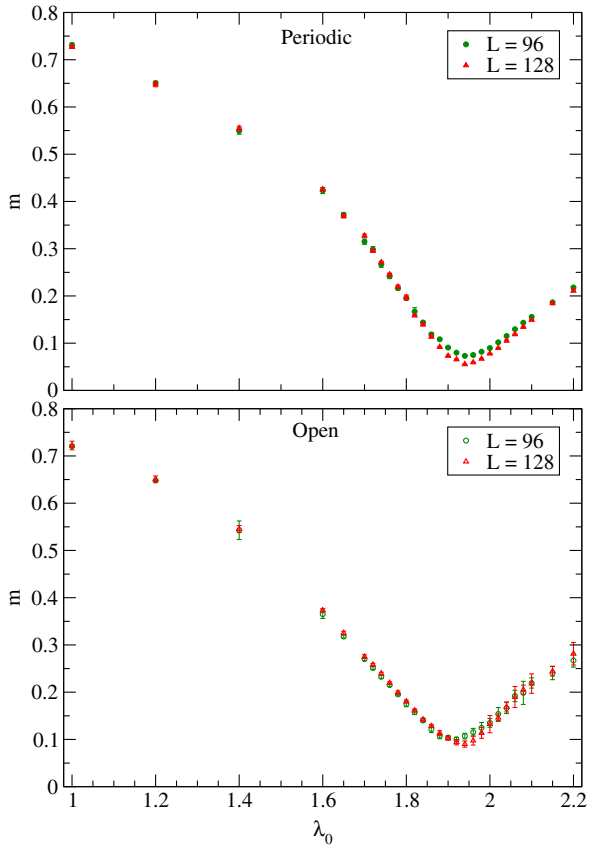

FIG. 16. The volume dependence of the boson mass versus λ_0 for PBC (top) and OPEN (bottom) at $m_0^2 = -0.5$.

system L, and the microscopic length a (lattice spacing)—the last one drops out near the critical region due to universality.

For any observable P_L computed on a lattice of finite extent L, the nonanalyticity near the critical point in the infinite-volume limit can be expressed in the form of a scaling law $P_\infty(\tau) = A_P \tau^{-\rho}$, where $\tau = (\lambda_0^c - \lambda_0)/\lambda_0^c$ and ρ is the critical exponent associated with the observable. Following the arguments of FSS analysis, it can be shown that

$$L^{\rho/\nu}/P_L(\tau) = A_P^{-1} A_\xi^{\rho/\nu}[C_P + D_P\, A_\xi^{-1/\nu}\tau L^{1/\nu} + \mathcal{O}(\tau^2)], \tag{17}$$

where ν is the critical exponent associated with the correlation length ξ. Equation (17) implies that if we plot $L^{\rho/\nu}/P_L(\tau)$ versus the coupling λ_0 for different values of L, all the curves will pass through the same point where $\tau = 0$, or equivalently $\lambda_0 = \lambda_0^c$ [26].

The critical behavior of $\langle\phi\rangle$, the susceptibility χ, and the mass gap $m = 1/\xi$ may be written as

$$\langle\phi\rangle = A_\phi^{-1}\tau^\beta, \qquad \chi = A_\chi \tau^{-\gamma}, \quad \text{and} \quad m = A_\xi^{-1}\tau^\nu. \tag{18}$$

From the general expectation that in $1+1$ dimensions ϕ^4 theory and the Ising model belong to the same universality class, we use the Ising values for the corresponding exponents as inputs in our FSS analysis. Thus, $\beta = 0.125$, $\gamma = 1.75$, and $\nu = 1$.

The plot of $\langle|\phi|\rangle L^{0.125}$ versus λ_0 for different values of gradient flow level at $m_0^2 = -0.5$ with a periodic boundary in the temporal direction is presented in Fig. 12. In spite of the fact that $\langle|\phi|\rangle$ changes with the gradient flow level, the critical coupling λ_0^c is found to be unaffected by gradient flow. The critical coupling λ_0^c is found to be a little less than 1.94 for $m_0^2 = -0.5$. A similar FSS analysis has been done at $m_0^2 = -1.0$, leading to the same conclusion along with an estimated value of $\lambda_0^c \approx 4.46$.

A similar FSS analysis of the susceptibility calculated at $m_0^2 = -0.5$ for various values of gradient flow level (for PBC) is presented in Fig. 13. Here, the smoothening effect of gradient flow has helped to pinpoint the location of the critical coupling λ_0^c which matches the estimate from the FSS analysis for $\langle|\phi|\rangle$. A similar FSS analysis done at $m_0^2 = -1.0$ also gives the corresponding value of λ_0^c which matches that obtained from the FSS analysis for $\langle|\phi|\rangle$.

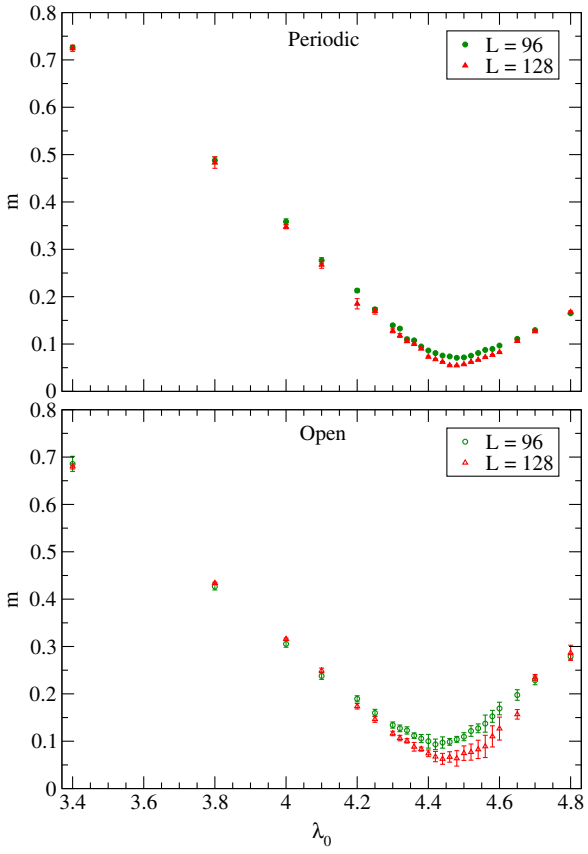

FIG. 17. The volume dependence of the boson mass versus λ_0 for PBC (top) and OPEN (bottom) at $m_0^2 = -1.0$.

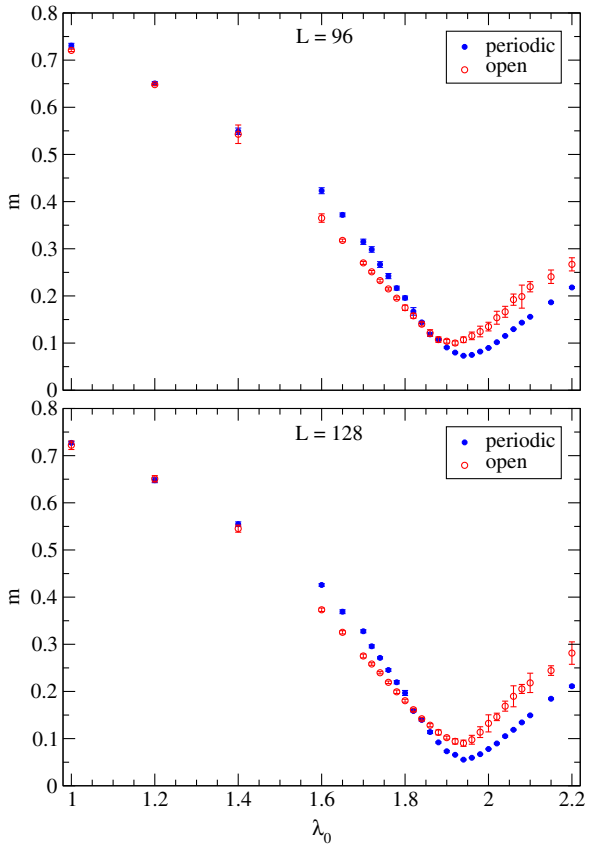

FIG. 18. The effect of the boundary condition on the boson mass versus λ_0 for $L = 96$ (top) and $L = 128$ (bottom) at $m_0^2 = -0.5$.

Using the same ansatz, we attempt an FSS analysis for both $\langle|\phi|\rangle$ and χ in the case of an open boundary in the temporal direction. The results are presented in Figs. 14 and 15, respectively. It is obvious from the figures that the critical point is not pinpointed as clearly as in the case of PBC. A strange pattern is found for the susceptibility, for which the curves with different L—instead of passing through a point—appear to overlap within statistical errors at and between the values 1.92 and 1.94 of λ_0. Anyway, the effect of the surface in the case of an open boundary needs to be included in the ansatz for finite-size scaling analysis. For that purpose a more precise numerical study is necessary, which is beyond the scope of this study.

D. The boson mass

Finally, in this subsection we present the results for the mass spectrum of the theory. The boson mass has been extracted from the plateau along the time direction for an effective mass which is computed from two-point and one-point correlation functions of the time-sliced scalar field $\phi(t)$ for PBC and OPEN, respectively. For this purpose, we first determine the gradient flow level for which the plateau for the effective mass is found to be the most stable one for each coupling (also for PBC and OPEN separately). The computation of the mass has been done only for the two largest lattices (namely, for $L = 96$ and $L = 128$) since, for the smaller lattices, the temporal extent is not sufficiently long to observe the decrease of the correlation function, particularly within the critical region. Because of this, it is not meaningful to perform the formal FSS analysis. However, even with lattices of only two different sizes, we observe a noticeable finite-volume effect.

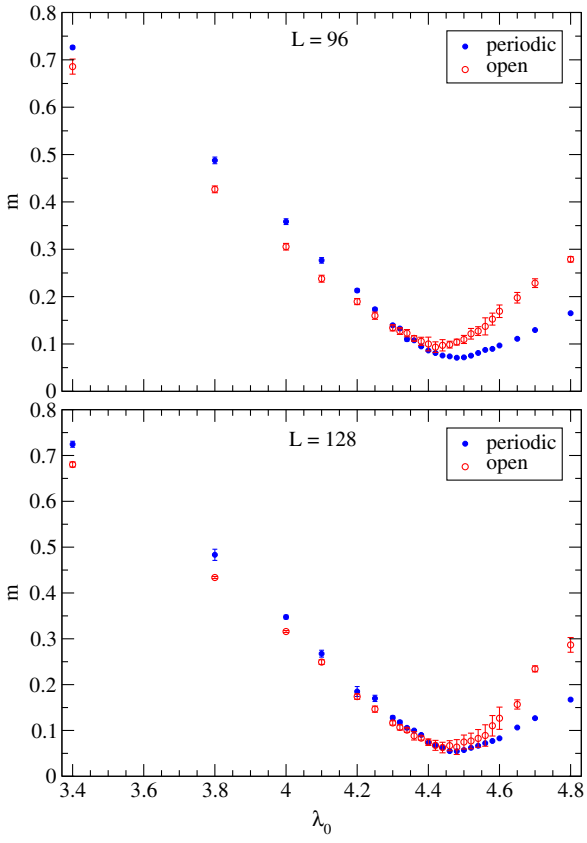

FIG. 19. The effect of the boundary condition on the boson mass versus λ_0 for $L = 96$ (top) and $L = 128$ (bottom) at $m_0^2 = -1.0$.

In Figs. 16 and 17 we compare the volume dependence of the boson mass versus λ_0 for periodic (top) and open (bottom) boundary conditions at $m_0^2 = -0.5$ and $m_0^2 = -1.0$, respectively. In the case of PBC the effect of the finite volume on the mass spectrum is clearly visible in the critical region, but for OPEN this effect is not that obvious from the respective figure. However, if we remember from the behaviors of $\langle|\phi|\rangle$ and χ that the phase transition point shifts towards the smaller values of λ_0 compared to PBC and that the shift is greater for smaller volumes, it appears that this leftward shift of the transition point has overshadowed the finite-volume effect.

The effects of the boundary on the mass spectrum have been demonstrated in Figs. 18 and 19 for two different values of the lattice mass parameters: $m_0^2 = -0.5$ and $m_0^2 = -1.0$, respectively. The leftward shift of the phase transition point is found to be almost diminishing for the larger lattice. The boundary effects are more prominent near the critical point, as evident from the clearly sharper nature of the transition in the case of PBC compared to that of OPEN.

VI. CONCLUSIONS

We have found the gradient flow to be very effective in reducing the unwanted lattice artifacts in the functional average of the time-sliced field $\phi(t)$, the susceptibility, and the extraction of boson mass from both two-point (PBC) and one-point (OPEN) correlators. We have shown that, in spite of the fact that $\langle|\phi|\rangle$ changes with gradient flow (the transition is more prominent with increasing flow level), the transition point does not depend on the gradient flow level. In the case of susceptibility, it was found that the increase in the level of gradient flow raises the height of the peak but leaves the peak position (the phase transition point for a given volume) practically unaltered. This behavior is consistent with the expectation that the gradient flow helps to reduce the lattice artifacts and brings the lattice theory closer to the continuum physics, where we expect the susceptibility to diverge as the critical point is approached. The critical coupling λ_0^c has been obtained for both $\langle|\phi|\rangle$ and χ from a detailed finite-size scaling analysis of the data for various lattice sizes and gradient flow levels; the results are qualitatively unchanged for different flow levels, but

they seem to be determined more clearly with a nonzero value for the flow level.

For all of the observables studied here, for a given volume, the phase transition point has a leftward shift in terms of λ_0 in the case of OPEN compared to PBC for a fixed value of m_0^2, and this leftward shift diminishes as the volume increases. In addition, for a given volume, the phase transition curve is found to be more prominent or sharp in the case of PBC compared to OPEN. In particular, noticeable boundary effects are observed on the mass spectrum in the critical region where the effects of the open boundary extend deep into the bulk region [as emphasized by the behavior of $\langle|\phi(t)|\rangle$] and the finite-volume artifacts become much more important compared to the case of the periodic boundary condition. An extensive analytical study of the boundary effects due to an open boundary in the critical region, taking into consideration the finite-size scaling, will be very fruitful.

The main objective of the present study has been to investigate the effects of the gradient flow and the open boundary condition in the temporal direction in a theory with a vanishing mass gap and without the complexities of renormalization. Since it is known that in $3+1$-dimensional ϕ^4 theory the straightforward use of the gradient flow equation leads to new divergences in correlation functions at nonzero flow time, a detailed comparison of various proposals to overcome this problem needs to be investigated. Our current study has demonstrated that in the region of vanishing mass gap, an open boundary introduces complexities when used in a lattice with finite volume. Our previous success with an open boundary in pure Yang-Mills theory may be partly due to the reasonably large mass gap (glueball mass) in this theory. On the other hand, the relevant mass gap of QCD (determined by the two-pion state) is much lower, and we expect an open boundary to have nontrivial consequences in the scaling region. This requires a thorough investigation in the future.

ACKNOWLEDGMENTS

To carry out all the numerical calculations reported in this work, the Cray XE6 system supported by the 11th-12th Five Year Plan Projects of the Theory Division, SINP under the Department of Atomic Energy, Government of India, was used. We thank Richard Chang for the prompt maintenance of the system.

[1] A. K. De, A. Harindranath, J. Maiti, and T. Sinha, Investigations in $1+1$ dimensional lattice ϕ^4 theory, Phys. Rev. D **72**, 094503 (2005).
[2] A. K. De, A. Harindranath, J. Maiti, and T. Sinha, Topological charge in $1+1$ dimensional lattice ϕ^4 theory, Phys. Rev. D **72**, 094504 (2005).
[3] M. Lüscher, Topology, the Wilson flow and the HMC algorithm, *Proc. Sci.*, LATTICE2010 (2010) 015, arXiv:1009.5877.
[4] M. Lüscher and S. Schaefer, Lattice QCD without topology barriers, J. High Energy Phys. 07 (2011) 036.
[5] M. Lüscher and S. Schaefer, Lattice QCD with open boundary conditions and twisted-mass reweighting, Comput. Phys. Commun. **184**, 519 (2013).
[6] A. Chowdhury, A. Harindranath, J. Maiti, and P. Majumdar, Topological susceptibility in lattice Yang-Mills theory with open boundary condition, J. High Energy Phys. 02 (2014) 045.
[7] A. Chowdhury, A. Harindranath, and J. Maiti, Open boundary condition, Wilson flow and the scalar glueball mass, J. High Energy Phys. 06 (2014) 067.
[8] A. Chowdhury, A. Harindranath, and J. Maiti, Correlation and localization properties of topological charge density and the pseudoscalar glueball mass in SU(3) lattice Yang-Mills theory, Phys. Rev. D **91**, 074507 (2015).
[9] A. Chowdhury, A. Harindranath, and J. Maiti, Physical observables from boundary artifacts: scalar glueball in Yang-Mills theory, J. High Energy Phys. 02 (2016) 134.
[10] A. Amato, G. Bali, and B. Lucini, Topology and glueballs in $SU(7)$ Yang-Mills with open boundary conditions, *Proc. Sci.*, LATTICE2015 (2015) 292, arXiv:1512.00806.
[11] M. Bruno *et al.*, Simulation of QCD with $N_f = 2+1$ flavors of non-perturbatively improved Wilson fermions, J. High Energy Phys. 02 (2015) 043.
[12] See, for example, N. Shibata and C. Hotta, Boundary effects in the density-matrix renormalization group calculation, Phys. Rev. B **84**, 115116 (2011).
[13] M. Lüscher, Trivializing maps, the Wilson flow and the HMC algorithm, Commun. Math. Phys. **293**, 899 (2010).
[14] M. Lüscher, Properties and uses of the Wilson flow in lattice QCD, J. High Energy Phys. 08 (2010) 071.
[15] M. Lüscher and P. Weisz, Perturbative analysis of the gradient flow in non-Abelian gauge theories, J. High Energy Phys. 02 (2011) 051.
[16] C. Monahan and K. Orginos, Locally smeared operator product expansions in scalar field theory, Phys. Rev. D **91**, 074513 (2015).
[17] K. Fujikawa, The gradient flow in $\lambda\phi^4$ theory, J. High Energy Phys. 03 (2016) 021.
[18] M. Dalla Brida, M. Garofalo, and A. D. Kennedy, Numerical stochastic perturbation theory and gradient flow

in ϕ^4 theory, *Proc. Sci.*, LATTICE2015 (2015) 309, arXiv:1512.08222.

[19] C. Monahan, The gradient flow in simple field theories, *Proc. Sci.*, LATTICE2015 (2015) 052, arXiv:1512.00294.

[20] I. Montvay and G. Munster, *Quantum Fields on a Lattice* (Cambridge University Press, Cambridge, England, 1997), p. 57.

[21] R. C. Brower and P. Tamayo, Embedded dynamics for ϕ^4 theory, Phys. Rev. Lett. **62**, 1087 (1989).

[22] U. Wolff, High precision simulation techniques for lattice field theory, Int. J. Mod. Phys. C **04**, 451 (1993).

[23] U. Wolff, Collective Monte Carlo updating for spin systems, Phys. Rev. Lett. **62**, 361 (1989).

[24] J. L. Cardy, in *Finite-Size Scaling*, edited by J. L. Cardy (Elsevier, New York, 1988).

[25] E. Brézin, An investigation of finite size scaling, J. Phys. II (France) **43**, 15 (1982); reprinted in Ref. [24].

[26] N. Goldenfeld, *Lectures on Phase Transitions and the Renormalization Group* (Addison-Wesley, Reading, MA, 1992).